AGU PUBLICATIONS

Geophysical Research Letters

RESEARCH LETTER
10.1002/2015GL063027

Key Points:
- We took the time-varying discharge rate of explosive eruptions into account
- We model volcanic ash dispersal including the variation of input parameters
- We compare model and lidar-derived concentration and the uncertainty

Correspondence to:
S. Scollo,
simona.scollo@ingv.it

Citation:
Scollo, S., A. Boselli, M. Coltelli, G. Leto, G. Pisani, M. Prestifilippo, N. Spinelli, and X. Wang (2015), Volcanic ash concentration during the 12 August 2011 Etna eruption, *Geophys. Res. Lett.*, *42*, 2634–2641, doi:10.1002/2015GL063027.

Received 5 JAN 2015
Accepted 18 MAR 2015
Accepted article online 24 MAR 2015
Published online 16 APR 2015

Volcanic ash concentration during the 12 August 2011 Etna eruption

Simona Scollo[1], Antonella Boselli[2], Mauro Coltelli[1], Giuseppe Leto[3], Gianluca Pisani[4], Michele Prestifilippo[1], Nicola Spinelli[4], and Xuan Wang[5]

[1]Istituto Nazionale di Geofisica e Vulcanologia, Osservatorio Etneo, Sezione di Catania, Catania, Italy, [2]CNISM and IMAA-CNR, Potenza, Italy, [3]INAF-Osservatorio Astrofisico di Catania, Catania, Italy, [4]CNISM and Dipartimento di Fisica, Università di Napoli "Federico II", Naples, Italy, [5]CNISM and CNR-SPIN, Dipartimento di Scienze Fisiche, Università di Napoli "Federico II", Naples, Italy

Abstract Mount Etna, in Italy, is one of the most active volcanoes in the world and an ideal laboratory to improve volcano ash monitoring and forecasting. During the volcanic episode on 12 August 2011, an eruption column rose up to several kilometers above sea level (asl), and the volcanic plume dispersed to the southeast. From the video-surveillance system, we were able to estimate variations in the column height (peak value of 9.5 ± 0.5 km above sea level) with time. We derived the time-varying discharge rate (peak value of $60\ m^3\ s^{-1}$) and determined the ash concentration using a volcanic ash dispersal model. The modeled ash concentration was compared with lidar measurements using different particle effective radius, and differences are within the error bars. Volcanic ash concentrations range from 0.5 to $35.5 \times 10^{-3}\ g\ m^{-3}$. The comparison highlights that to improve volcanic ash forecasting during volcanic crises it is necessary to take into account the time-varying discharge rate of explosive eruptions.

1. Introduction

On the morning of 12 August 2011, the New South East Crater of Etna volcano (Italy) produced the tenth event of the 2011–2012 eruptive sequence. The eruption generated a powerful lava fountain, during the most intense phase, forming a several kilometer high eruption column (Figure 1a). Volcanic ash dispersal simulations, running daily at the Istituto Nazionale di Geofisica e Vulcanologia, Osservatorio Etneo (INGV-OE), forecasted that the volcanic plume dispersal was to the southeast. Nevertheless, the features of the 12 August 2011 lava fountain event differed from those used in running the daily simulations [*Scollo et al.*, 2009]; and consequently, the modeled ash concentration may have been different from the actual ash. The 12 August 2011 event features were similar to that of lava fountains occurring in the year 2000 [*Alparone et al.*, 2007] while they differed from the 1998 [*Scollo et al.*, 2008], the 2001 [*Scollo et al.*, 2007], and 2002–2003 eruptions [*Andronico et al.*, 2008]. For those events, the eruption source parameters needed by volcanic ash dispersal models were accurately identified and are used as reference scenarios to run the daily simulations [*Scollo et al.*, 2009]. The use of eruptive scenarios is applied worldwide and is an effort to improve the accuracy of simulations in the early hours of an eruption [*Mastin et al.*, 2009], though the limitations of this are well known owing to the unpredictability of the future eruptions [*Folch*, 2012]. In this paper, we first make an attempt to take the evolution with time into account.

The frequent explosive activity has prompted the INGV-OE to improve its volcanic plume monitoring and forecasting system through the introduction of new remote sensing techniques that can collect data in near real time [*Scollo et al.*, 2012; *Pisani et al.*, 2012; *Scollo et al.*, 2014]. The biggest limitation in forecasting the volcanic plume dispersal is the lack of rapidly available direct observations in the initial stage and during an eruption that may be used to run numerical simulations [*Bonadonna et al.*, 2012]. The INGV-OE monitors the activity of Sicilian volcanoes through a video-surveillance system made up of visible and thermal cameras that at the time of the eruption were located in Catania (ECV), Milo (EMV), Nicolosi (ENV and ENT), Schiena dell'Asino (ESV), and La Montagnola (EMOV and EMOT) (Figure 1b). Recently, *Scollo et al.* [2014] proposed a method to estimate the column height by combining wind forecasts and images of the ECV camera. In this paper, we demonstrate that the combination of ground-based video surveillance and lidar systems may substantially improve the measurement of volcanic particles and that leads toward a reliable quantification of volcanic ash concentration in the atmosphere. We use the observations of the column height (CH) obtained

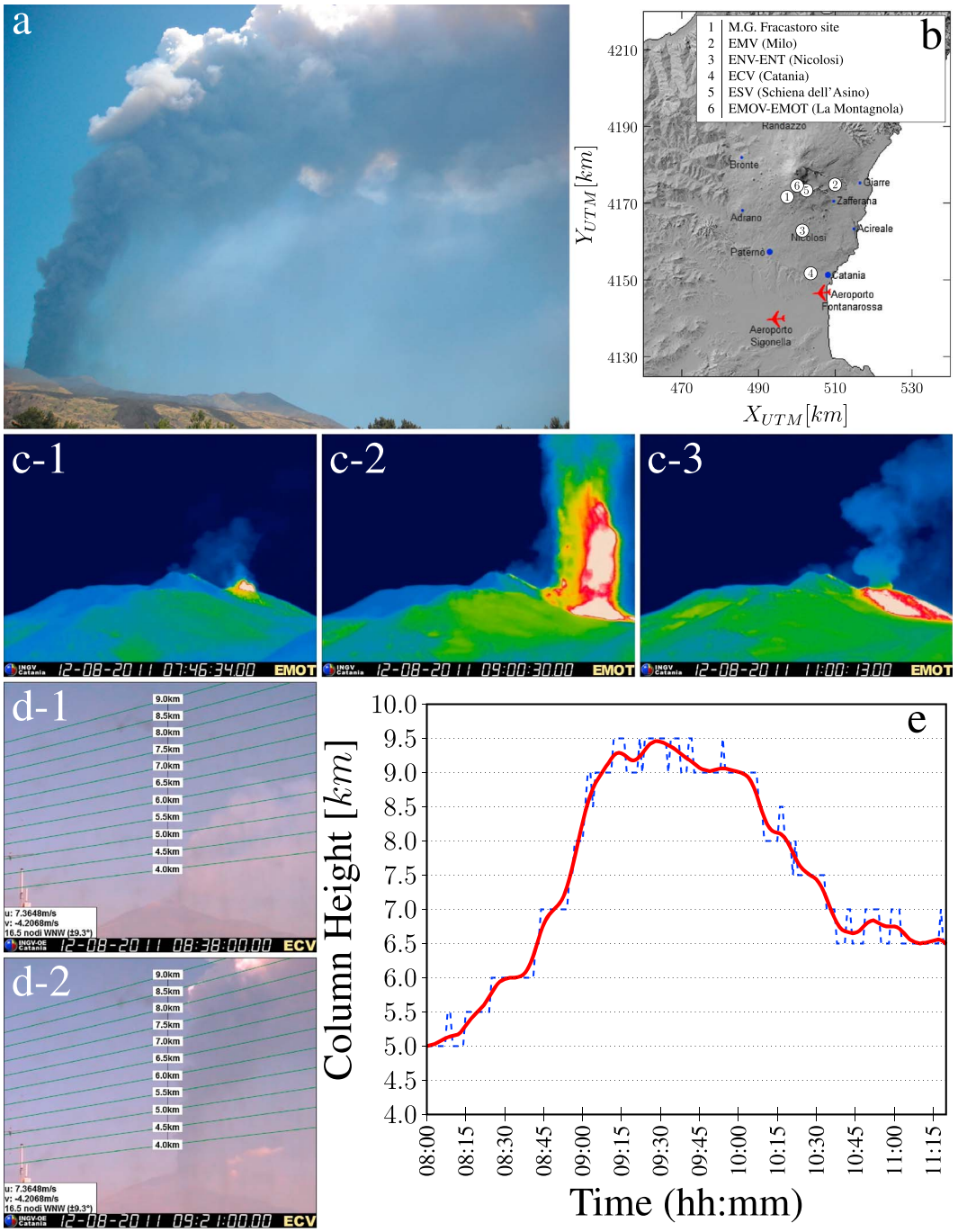

Figure 1. (a) Photo of the 12 August 2011 eruption column taken by S.Scollo at the M.G. Fracastoro site of the Istituto Nazionale di Astrofisica; (b) map including all the locations reported in the paper. Eruptive activity seen by EMOT of (c-1) Phase 1; (c-2) Phase 2; (c-3) Phase 3; images of the ECV camera used to estimate the column height at (d-1) 08:38 UTC and (d-2) 09:21 UTC using the method proposed by *Scollo et al.* [2014]; and (e) variation of the column height with 5 min time steps (blue line) and variation of the column height with 5 min time steps using a low-pass filter (red line) obtained by the analysis of the ECV images.

by the video-surveillance images to evaluate in near real time the time variations of mass eruption rate (MER) and include both eruption source parameters in the modeling. Volcanic ash concentrations obtained by computer simulations are then compared with those estimated by a scanning lidar system [*Scollo et al.*, 2012]. For the first time at Etna, we have been able to quantify the volcanic ash concentrations in the atmosphere.

This study may help quantify the impact that Etna's lava fountains have on aviation safety to prevent the flights in the areas of high contamination ($>4\times10^{-3}$ g/m^3) in compliance with the International Civil Aviation Organization directives [*International Civil Aviation Organization* (*ICAO*), 2010].

2. The 12 August 2011 Paroxysm

The 12 August 2011 lava fountain event was preceded by an increase in the amplitude of volcanic tremor several hours before the onset of the paroxysmal phase [*D'Agostino et al.*, 2013]. Sporadic ash emissions came early the strombolian activity that intensified from about 05:30 to 07:30 UTC, while at the same time there was a gradual increase in volcanic tremor [*D'Agostino et al.*, 2013]. After 07:30 UTC, strombolian explosions produced dark ash puffs (Figure 1c-1, *Phase 1*), and a lava flow was emitted at the base of the cone at 07:50 UTC toward the Valle del Bove [*Behncke et al.*, 2014]. The activity increased in frequency and intensity progressing from violent strombolian explosions to a sustained lava fountain at about 08:30 UTC [*D'Agostino et al.*, 2013]. The eruption column rose high above the vent between 08:45 and 10:00 UTC (Figure 1c-2, *Phase 2*), and after 10:30 UTC, the activity decreased and completely ceased around 11:00 UTC (Figure 1c-3, *Phase 3*). After the end of the activity, the lava flow reached a length of 2.9 km, the volume was estimated between 1.29×10^6 and 2.20×10^6 m^3 with a mean effusion rate of 323 m^3/s [*Behncke et al.*, 2014]. The volcanic plume dispersed toward the southeast; tephra fell on the towns of Zafferana and Milo, and as far as the Ionian coast covering a wide area between Giarre and Acireale towns (Figure 1b).

3. Column Height Estimation by the ECV Camera

We applied the method of *Scollo et al.* [2014] to the 12 August 2011 event for evaluating the column height with a resolution of ± 500 m. The method consisted of estimating (i) the intrinsic parameters of the ECV camera, (ii) the full camera model to locate any image point in the space of the camera field of view, (iii) the geometry of the plume considering the vertical plane passing through the volcanic vent and parallel to the mean wind direction. The eruptive activity began to intensify at 08:30 UTC, and the column rose to 6.0 ± 0.5 km asl, remaining constant up to about 08:40 UTC (Figure 1d-1) and then increased by about 1 km in only 5 min (08:45 UTC). The ECV camera retrieved the value of 9.0 ± 0.5 km asl between 09:00 and 10:00 UTC (Figure 1d-2). Figure 1e shows the variation of the column height (asl) with a time step of 5 min. At the beginning of the lava fountain, the column rose up to 5.0 ± 0.5 km asl. The activity slowly decreased, and the column descended to 8.0 km altitude asl at 10:22 UTC, and then to 6.5 ± 0.5 km asl at 10:30 UTC, maintaining this height until the end of the eruptive activity.

4. Lidar Measurements

Volcanic ash measurements were carried out by the Volcanic Ash Monitoring by Polarization lidar system installed at the M.G. Fracastoro site (14.97E, 37.69 N) of the Istituto Nazionale di Astrofisica, 7 km away from Etna's summit craters. The backscatter coefficient profile was obtained by the lidar measurements using the Klett-Fernald algorithm [*Fernald*, 1984; *Klett*, 1985]. The lidar ratio (LR) inside the plume was assumed of about 36 sr, as described in *Pisani et al.* [2012]. The calibrated particle linear depolarization values in the plume were obtained from the ratio of the power measured in the parallel and perpendicular polarized channels. The angular misalignment of the receiving optics was also taken into account [*Pisani et al.,* 2012]. The contribution of background aerosol load was considered negligible, less than ~ 10^{-7} sr^{-1} m^{-1} in the Mediterranean region in clear-sky conditions [*Sicard et al.*, 2011].

Lidar measurements were carried out from 08:59 to 11:56 UTC. Figure 2a-1 shows the aerosol backscattering coefficient values (βaer) and the aerosol depolarization profiles (δaer) obtained from the measurements performed by pointing the laser beam toward the plume for 10 min (09:01–09:11 UTC) and when the eruption column (at 09:01 UTC) reached the height of 9 ± 0.5 km (Figure 2a-2). Lidar profiles showed two layers with different properties. The first layer (Layer 1), between 5.5 and 6.1 km from the lidar station along the laser beam, was characterized by lower βaer (~0.15×10^{-5} m^{-1} sr^{-1}) and δaer ~ 5%. The second layer (Layer 2) located between 6.2 and 6.8 km was characterized by peak values of βaer around 1×10^{-4} m^{-1} sr^{-1} and δaer of about 20%, suggesting that volcanic ash was mainly contained in this layer. Figure 2b shows the map of βaer measured starting from 10:22 to 10:28 UTC with an integration step of 60 s. In order to probe the volcanic plume, the scanning was performed by changing the lidar elevation between 20° and 59° in elevation with a

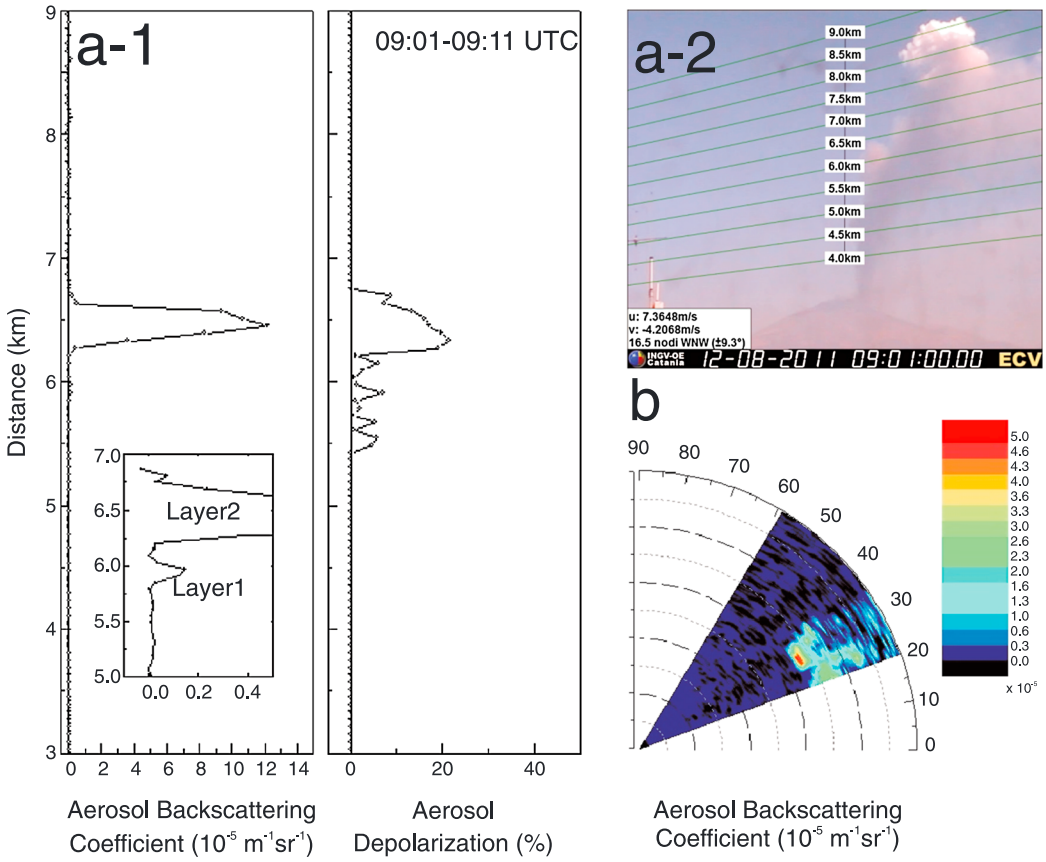

Figure 2. (a-1) Aerosol backscattering and aerosol depolarization profiles measured at Serra la Nave station on 12 August 2011. Data started at 09:01 UTC and were acquired for 10 min with an integration time of 60 s; (a-2) ECV image showing the column height between 8.5 and 9 km asl at 09:01 UTC; and (b) particle backscattering (m^{-1} sr^{-1}) from 10:22 to 10:28 UTC of the scanning measurements, with elevations between 20° and 59° and azimuth of 36.7°. Integration time was 60 s.

fixed azimuth of 36.7°. The volcanic particles were located between 6.5 km and 8.0 km from the lidar station along the laser beam, in agreement with a column height of about 7.5 km asl estimated by the video-surveillance images recorded between 10:22 and 10:28 UTC. Inside the plume, the mean value of βaer was about $2\times10^{-5}\,m^{-1}\,sr^{-1}$ and reached the maximum value of about $5\times10^{-5}\,m^{-1}\,sr^{-1}$ at 30.4°, about 6.5 km from the lidar station along the laser beam.

5. Ash Concentration Estimation

Volcanic ash concentration in the air was simulated using the Lagrangian numerical model named PUFF [*Searcy et al.*, 1998; *Tanaka and Yamamoto*, 2002; *Webley et al.*, 2008]. We made some changes to the original code and applied a statistical procedure to evaluate ash concentrations in the atmosphere [*Scollo et al.*, 2011]. For the first time at Etna, we took the time variations in the eruptive activity into account. In the simulations, we included the variations of both column heights (CH) retrieved by the ECV camera (Figure 1d) and the mass eruption rates (MER) obtained by applying the relationship $CH = 0.3035\times MER^{0.241}$ [*Mastin et al.*, 2009]. The total grain size distribution was assumed constant for all the runs and equal to values reported in *Andronico et al.* [2014] that are suitable for lava fountain events occurring between 2011 and 2012. This distribution peaked at -3φ ($\varphi = -\log_2(d)$ where d is the particle diameter in mm), has a median value of -1.4φ, and was extrapolated using an exponential fit to take into account the contribution of particles up to 8φ (~ 4 μm). The percentage of the fine particles (<30 μm) was ~ 1.5%, consistent with values reported from *Gurrieri et al.* [2015]. We ran 28 different simulations that all began at 08:30 UTC and ended at 11:30 UTC. Each simulation had only one 5 min eruption that occurred between 08:30 and 10:45 UTC and was constrained with the MER from the EVC camera. The simulations were then summed together to encompass the total eruption duration

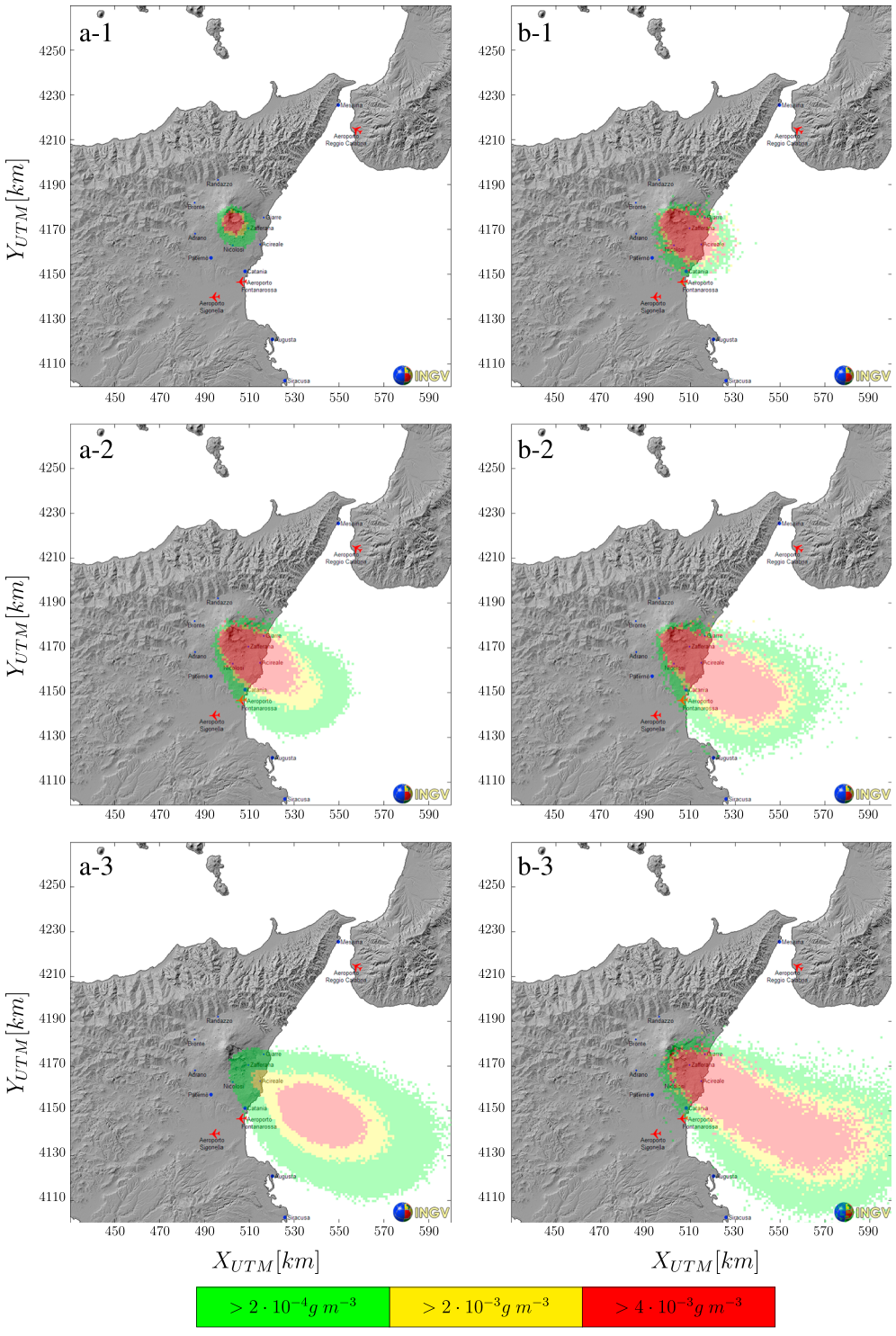

Figure 3. Volcanic ash concentration map plotted at 7 km asl and computed by the PUFF model using a variable mass eruption rate at (a-1) 09:00 UTC, (a-2) 10:00 UTC, and (a-3) 11:00 UTC and a constant mass eruption rate at (b-1) 09:00 UTC, (b-2) 10:00 UTC, and (b-3) 11:00 UTC.

and the mass ash concentration in the atmosphere at any specific time. The end time of each simulation was set to 11:30 UTC. The results of each simulation were summed to estimate the mass ash concentration in the air at any specific time. In agreement with *Scollo et al.* [2011], the number of particles used in the simulations was 5 millions while the time step was set to 1 min. For example, the PUFF result at 10:05 UTC is

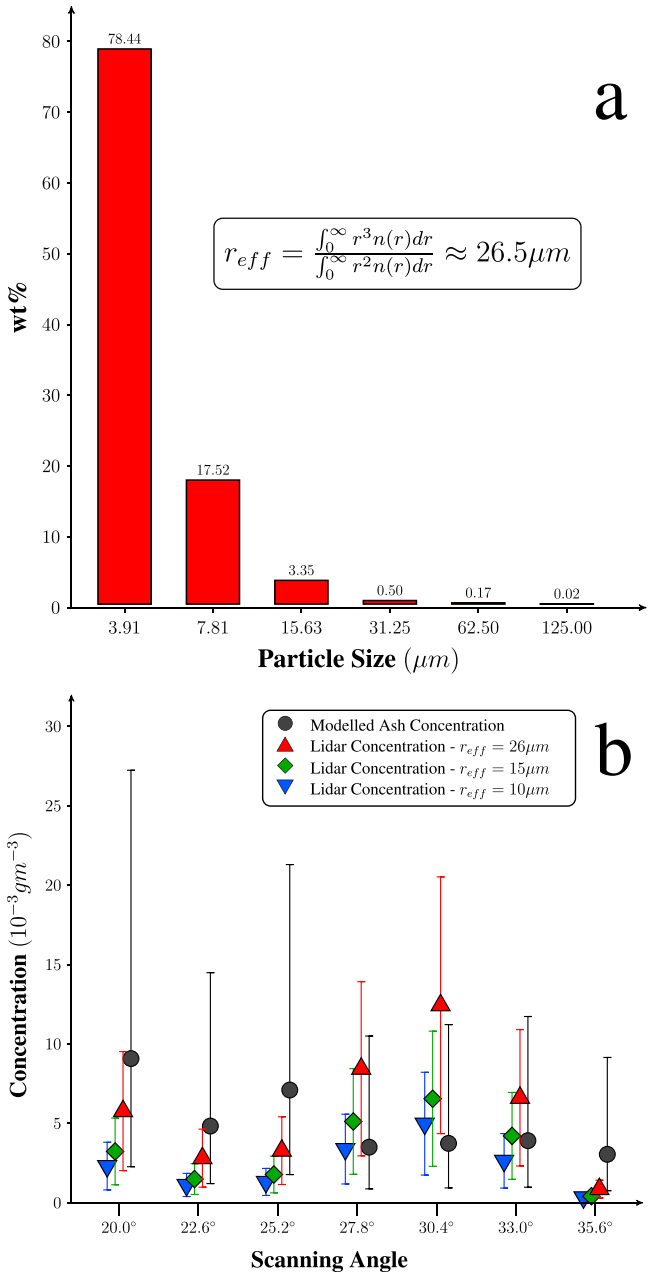

Figure 4. (a) Particle size distribution obtained from the PUFF model inside the region investigated by lidar, and (b) comparisons between volcanic ash concentration computed and measured by lidar using three different effective radius (r_{eff}). Error bar for the modeled ash concentration is related to the MER error; error bar for the lidar ash concentration is set to 55%.

given by the sum of all the simulations between 08:30 and 10:00 UTC. Meteorological data were provided by the Italian Air Force Meteorological Office and Italian National Department of Civil Protection, and covered the entire area of Sicily [*Scollo et al.*, 2009]. The PUFF results at 09:00, 10:00, and 11:00 UTC for 7 km asl using a variable MER (Figures 3a-1–Figure 3a-3) and a constant MER (Figure 3b-1–Figure 3b-3) are shown for comparison. The ash concentration thresholds are 2×10^{-4}, 2×10^{-3}, and 4×10^{-3} g m^{-3} [*ICAO*, 2010]. Simulations clearly show that Etna's eastern and south eastern flanks are affected by volcanic ash dispersal and that after 11:00 UTC the ash concentration was less than 2×10^{-4} g m^{-3}. The simulations using a constant MER computed a wider area affected by ash at the beginning and end of the explosive activity. If the volcanic cloud had expanded above the eastern flight zone, it would have been dangerous for aviation safety. We compared the results of simulations with lidar measurements retrieved between 10:22 and 10:28 UTC. Ash concentrations from lidar measurements were obtained following the approach described in *Pisani et al.* [2012] and *Scollo et al.* [2012]. First, we evaluated the ash-related backscatter coefficient βa following the method proposed by *Tesche et al.* [2009]:

$$\beta_a = \beta_{aer} \frac{(\delta_{aer} - \delta_{na})(1 + \delta_a)}{(\delta_a - \delta_{na})(1 + \delta_{aer})}$$

where βaer and δaer values are the aerosol backscatter and depolarization coefficients obtained by lidar measurements, δna and δa are the depolarization ratio coefficients of the depolarizing ash and of the weakly depolarizing nonash aerosol, and are set to 0.01 and 0.5. Then we obtained the volcanic ash concentration c by

$$c = k \times LR \times \rho \times \beta_a$$

where k is the ash conversion factor which is a function of the effective particle radius r_{eff} ($k = 2/3\ r_{eff}$). LR is the mean value of the estimated lidar ratio, ρ is the density of volcanic ash fixed to 2450 kg/m^3, and β_a is the ash-related backscatter coefficient [*Pisani et al.*, 2012]. We evaluate the lidar concentrations using three different r_{eff}. The r_{eff} was set to 10 μm and 15 μm consistent with values reported by *Guerrieri et al.*

[2015] and set to 26 μm obtained by simulations computed by PUFF in the same area investigated by lidar (Figure 4a):

$$r_{\text{eff}} = \frac{\int_0^\infty r^3 n(r)\mathrm{d}r}{\int_0^\infty r^2 n(r)\mathrm{d}r}$$

where r is the particle radius and $n(r)$ is the number density per unit radius [*Stevenson et al.*, 2015].

Figure 4b shows the comparisons between the modeled ash concentration and the lidar-derived concentration for three different particle sizes (10, 15, and 25 μm). Following *Pisani et al.* [2012], error on ash mass concentration obtained by lidar is evaluated from statistical uncertainties of βa, LR, and ρ resulting in the order of 55%. Error in ash mass concentration estimated by modeling is related to the fact that the equation of *Mastin et al.* [2009] has an inherent accuracy and uncertainty to a factor of 2. Results show that the modeled ash concentrations are comparable with those obtained by lidar for three different particle sizes. Lidar measurements reflected the pulsating nature of the lava fountain activity (high-frequency magma jet forming a fairly constant eruption column) that was not simulated in the modeling because the MER was set constant inside 5 min.

6. Discussion

The estimation of eruption source parameters during an eruption is a challenge that volcano observatories and scientific communities should pursue and make available to the Volcanic Ash Advisory Centre (VAAC). The main uncertainties of eruption source parameters are due to variations of eruption column height, mass eruption rate, total grain size distribution, and meteorological data [*Scollo et al.*, 2008; *Mastin et al.*, 2009; *Webley et al.*, 2009; *Bonadonna et al.*, 2012]. The combination of volcanological observations and modeling has allowed, for the first time at Etna volcano, to evaluate the volcanic ash concentration in the atmosphere and the degree of its uncertainty during the 12 August 2011 event.

The methodology presented in this work highlights different aspects. The measurement of eruption column height, in fine weather conditions, may be obtained by an inexpensive video-surveillance system [*Scollo et al.*, 2014]. Therefore, MER may be obtained by the well-known formulation that links it to the column heights. It should be noted that, for this eruption, the effect of the wind was negligible since the eruption occurred in low-wind condition ($<$10 m/s), and the values of MER are similar to those obtained by models taking account of the wind speed [e.g., *Degruyter and Bonadonna*, 2013]. Furthermore, the MER values show reasonable agreement with those obtained applying the 1-D dimensional model that takes into account effects of water, condensation, and ice formation on plume dynamics, as well as the effect of water added to the plume at the vent [*Mastin*, 2007].

During volcanic eruptions, column height is important to evaluate the area that may be affected by volcanic ash and forecast the region that should be avoided by aircraft [e.g., *Tupper et al.*, 2009]. The value of column height usually represents the maximum height reached by the plume. It is noteworthy that, depending on the eruption style, the column may reach the maximum height for a period less than the total eruption duration. In our study, the maximum column height ($\geq$9 km) was between 09:02 and 10:07 UTC, about half of the duration of the explosive phase. Consequently, the area affected by ash ($>2\times10^4$ g m^{-3}) computed by models that consider a constant column height for the entire eruptive period will be greater than the area that should be if the variable column height is taken into account. The use of time-varying mass eruption rate estimated by ground-based observations coupled with a volcanic ash dispersal model could reduce this gap and will have a closer match to the eruption's mass ash concentration obtained considering a constant eruption rate.

Our analysis could help the VAAC to improve forecasts and hazard assessments during an eruption, but the following three important steps are still needed: (i) improvement of the column height retrieval, while images may be generated during the eruption in less than 5 min, the values of column height are checked by the operator who may take up to an hour for the analysis; (ii) rapid communication among volcano observatories and VAACs, meaning enhanced collaboration among different agencies; and (iii) improvement of computing time. We take about 3 h to run our simulations, but the use of clusters could considerably reduce the time needed to run thousands of simulations. Furthermore, some researchers have suggested using probabilistic approaches [*Madankan et al.*, 2014] which could replace the existing deterministic approaches

[e.g., *Witham et al.,* 2007; *Webley et al.,* 2008]. We believe that probabilistic approaches may be applied during an impending eruption when data on eruption source parameters are not available. Greater efforts should nonetheless be made to render observations accessible to inverse approaches [*Stohl et al.*, 2011] so that decision makers have reliable information during volcanic emergencies.

Acknowledgments

We are grateful to the Italian Air Force Meteorological Office and Italian National Department of Civil Protection for providing meteorological data covering the entire area of Sicily on a daily basis. The authors thank C. Connor and K. Kiyosugi for suggesting some improvements to the PUFF code, C. Bonadonna and A. Costa for their valuable comments, Peter Webley and an anonymous reviewers that greatly helped to improve the quality of the paper. Video-surveillance images from the Istituto Nazionale di Geofisica e Vulcanologia, Osservatorio Etneo (INGV-OE) are subject to INGV data policy. Column height and lidar data reported in the paper and changes of the PUFF code necessary to reproduce our analysis are available from the authors upon request (simona.scollo@ingv.it). Sincere thanks go to Stephen Conway for helping with the English text. This study was undertaken by the MEDSUV project funded from the European Union's Seventh Programme for research, technological development, and demonstration under grant agreement 308665.

The Editor thanks Peter Webley and an anonymous reviewer for their assistance in evaluating this paper.

References

Alparone, S., D. Andronico, T. Sgroi, F. Ferrari, L. Lodato, and D. Reitano (2007), Alert system to mitigate tephra fallout hazards at Mt. Etna Volcano, Italy, *Nat. Hazards*, *43*, 333–350.

Andronico, D., S. Scollo, S. Caruso, and A. Cristaldi (2008), The 2002–03 Etna explosive activity: Tephra dispersal and features of the deposits, *J. Geophys. Res.*, *113*, B04209, doi:10.1029/2007JB005126.

Andronico, D., S. Scollo, A. Cristaldi, and M. D. Lo Castro (2014), Representivity of incompletely sampled fall deposits in estimating eruption source parameters: A test using the 12–13 January 2011 lava fountain deposit from Mt. Etna volcano, Italy, *Bull. Volcanol.*, *76*, doi:10.1007/s00445-014-0861-3.

Behncke, B., S. Branca, R. A. Corsaro, E. De Beni, L. Miraglia, and C. Proietti (2014), The 2011–2012 summit activity of Mount Etna: Birth, growth and products of the new SE crater, *J. Volcanol. Geotherm. Res.*, *270*, 10–21.

Bonadonna, C., A. Folch, S. Loughlin, and H. Puempel (2012), Future developments in modelling and monitoring of volcanic ash clouds: Outcomes from the first IAVCEI-WMO workshop on Ash Dispersal Forecast and Civil Aviation, *Bull. Volcanol.*, *74*, 1–10.

D'Agostino, M., G. Di Grazia, F. Ferrari, H. Langer, A. Messina, D. Reitano, and S. Spampinato (2013), Volcano monitoring and early warning on Mt. Etna, Sicily, based on volcanic tremor: Methods and technical aspects, in *Complex Monitoring of Volcanic Activity*, edited by V. M. Zobin, pp. 53–92, Nova Science, Hauppauge, N. Y.

Degruyter, W., and C. Bonadonna (2013), Impact of wind on the condition for column collapse of volcanic plumes, *Earth Planet. Sci. Lett.*, *377*, 218–226.

Fernald, F. G. (1984), Analysis of atmospheric lidar observations: Some comments, *Appl. Optic.*, *23*, 652–653.

Folch, A. (2012), A review of tephra transport and dispersal models: Evolution, current status, and future perspectives, *J. Volcanol. Geoth. Res.*, *235*, 96–115.

Guerrieri, L., L. Merucci, S. Corradini, and S. Pugnaghi (2015), Evolution of the 2011 Mt. Etna ash and SO2 lava fountain episodes using SEVIRI data and VPR retrieval approach, *J. Volcanol. Geotherm. Res.*, *291*, 63–71.

International Civil Aviation Organization (ICAO) (2010), Volcanic Ash Contingency Plan—Eur and Nat Regions, EUR Doc 019–NAT Doc 006, Part II, International Civil Aviation Authority.

Klett, J. D. (1985), Lidar inversion with variable backscatter/extinction ratios, *Appl. Optic.*, *24*, 1638–643.

Madankan, R., et al. (2014), Computation of probabilistic hazard maps and source parameter estimation for volcanic ash transport and dispersion, *J. Comput. Phys.*, *271*, 39–59.

Mastin, L. G. (2007), A user-friendly one-dimensional model for wet volcanic plumes, *Geochem. Geophys. Geosyst.*, *8*, doi:10.1029/2006GC001455.

Mastin, L. G., et al. (2009), A multidisciplinary effort to assign realistic source parameters to models of volcanic ash-cloud transport and dispersion during eruptions, *J. Volcanol. Geotherm. Res.*, *186*, 10–21.

Pisani, G., A. Boselli, M. Coltelli, G. Leto, G. Pica, S. Scollo, N. Spinelli, and X. Wang (2012), Lidar depolarization measurement of fresh volcanic ash from Mt. Etna, Italy, *Atmos. Environ.*, *62*, 34–40.

Scollo, S., P. Del Carlo, and M. Coltelli (2007), Tephra fallout of 2001 Etna flank eruption: Analysis of the deposit and plume dispersion, *J. Volcanol. Geotherm. Res.*, *160*, 147–164.

Scollo, S., S. Tarantola, C. Bonadonna, M. Coltelli, and A. Saltelli (2008), Sensitivity analysis and uncertainty estimation for tephra dispersal models, *J. Geophys. Res.*, *113*, doi:10.1029/2006JB004864.

Scollo, S., M. Prestifilippo, G. Spata, M. D'Agostino, and M. Coltelli (2009), Monitoring and forecasting Etna volcanic plumes, *Nat. Hazards Earth Syst. Sci.*, *9*, 1573–1585.

Scollo, S., M. Prestifilippo, M. Coltelli, R. A. Peterson, and G. Spata (2011), A statistical approach to evaluate the tephra deposit and ash concentration from PUFF model forecasts, *J. Volcanol. Geotherm. Res.*, *200*, 129–142.

Scollo, S., A. Boselli, M. Coltelli, G. Leto, G. Pisani, N. Spinelli, and X. Wang (2012), Monitoring Etna volcanic plumes using a scanning lidar, *Bull. Volcanol.*, *74*, 2382–2395, doi:10.1007/s00445-012-0669-y.

Scollo, S., M. Prestifilippo, E. Pecora, S. Corradini, L. Merucci, G. Spata, and M. Coltelli (2014), Height estimation of the 2011-2013 Etna lava fountains, *Ann. Geophys.*, *57*, doi:10.4401/ag-6396.

Searcy, C., K. Dean, and W. Stringer (1998), PUFF: A high-resolution volcanic ash tracking model, *J. Volcanol. Geotherm. Res.*, *80*, 1–16.

Sicard, M., F. Rocadenbosch, M. N. M. Reba, A. Comeron, S. Tomas, D. Garcia-Vizcaino, O. Batet, R. Barrios, D. Kumar, and J. M. Baldasano (2011), Seasonal variability of aerosol optical properties observed by means of a Raman lidar at an EARLINET site over Northeastern Spain, *Atmos. Chem. Phys.*, *11*, 175–190.

Stevenson, J. A., S. C. Millington, F. M. Beckett, G. T. Swindles, and T. Thordarson (2015), Big grains go far: Reconciling tephrochronology with atmospheric measurements of volcanic ash, *Atmos. Meas. Tech. Discuss.*, *8*, 65–120.

Stohl, A., et al. (2011), Determination of time- and height-resolved volcanic ash emissions and their use for quantitative ash dispersion modeling: The 2010 Eyjafjallajokull eruption, *Atmos. Chem. Phys.*, *11*, 4333–4351.

Tanaka, H. L., and K. Yamamoto (2002), Numerical simulation of volcanic plume dispersal from Usu Volcano in Japan on 31 March 2000 using PUFF model, *Earth Planets Space*, *54*, 743–752.

Tesche, M., A. Ansmann, D. Müller, D. Althausen, R. Engelmann, V. Freudenthaler, and S. Groß (2009), Separation of dust and smoke profiles over Cape Verde by using multiwavelength Raman and polarization lidars during SAMUM 2008, *J. Geophys. Res.*, *114*, D13202, doi:10.1029/2009JD011862.

Tupper, A., C. Textor, M. Herzog, A. F. Graf, and M. S. Richards (2009), Tall clouds from small eruptions: The sensitivity of eruption height and fine ash content to tropospheric instability, *Nat. Hazards*, *51*, 375–401.

Webley, P. W., K. Dean, J. E. Bailey, J. Dehn, and R. Peterson (2008), Automated forecasting of volcanic ash dispersion utilizing virtual globes, *Nat. Hazards*, doi:10.1007/s11069-008-9246-2.

Webley, P. W., B. J. B. Stunder, and K. G. Dean (2009), Preliminary sensitivity study of eruption source parameters for operational volcanic ash cloud transport and dispersion models—A case study of the August 1992 eruption of the Crater Peak vent, Mount Spurr, Alaska, *Volcanol. Geotherm. Res.*, *186*, 108–119.

Witham, C. S., M. C. Hort, R. Potts, R. Servranckx, P. Husson, and F. Bonnardot (2007), Comparison of VAAC atmospheric dispersion models using the 1 November 2004 Grimsvotn eruption, *Meteorol. Appl.*, *14*, 27–38.